In-Plane Micropump: Design Optimization

J. Sin, W.H. Lee and H.E. Stephanou

Center for Automation Technologies
CII 8015, 110 8th Street
Troy, New York, USA, sinj@cat.rpi.edu

ABSTRACT

This paper presents the fabrication, analysis and optimization of a novel monolithically fabricated diaphragm micropump, referred to as an in-plane micropump. Compared to previous technology, the micropump in this paper is fabricated to have all necessary components in a single silicon layer. The actuation principle is electrothermal expansion of a silicon V-beam, and its expansion is amplified through a lever structure to create a greater diaphragm stroke. Either a check valve or a diffuser is incorporated with a diaphragm to direct fluid flow. The Deep RIE (Reactive Ion Etching) process is used to fabricate the pump structure on a SOI (Silicon On Insulator) wafer, and the electromechanical property of the pump structure is characterized to estimate the pump's performance. Considering that minimization of energy consumption is one of the critical design objectives in micropumps, the design parameters of the pump structure are optimized for minimal driving power.

Keywords: micropump, electrothermal, modeling, power, optimization

1 INTRODUCTION

Micropumps play a key role in microfluidic circuits where nano or pico-liter volumes of fluid are delivered and controlled. Low cost and low driving power are important characteristics in addition to precision and miniaturization in hand-held applications on biotechnology, drug discovery and drug delivery. In general, diaphragm driven pumps have self-priming advantages compared to electrically driven pumps, and a variety of actuation principles, valve mechanisms and fabrication processes have been used to build diaphragm pumps [1]–[4]. Most existing pump designs consist of multiple layers, where each layer has a unique function, such as a diaphragm, a valve, or an actuator. However, multiple layer structures require expensive wafer alignment and bonding as well as externally assembled actuators, for example, piezoelectric disks.

Monolithic design reduces fabrication complexity, and also allows a small diaphragm and a pump chamber therefore precision control of flow rate can be possible. In the silicon micropump presented here, electrothermal actuators are embedded. Electrothermal expansion provides higher force compared to electrostatic methods, but in practice the stroke is not sufficient to achieve the desired compression ratio. A high power source can generate larger stroke but the trade off is higher energy consumption. For this reason, we adopt a stroke amplification mechanism to design pump actuation structures. An important goal is to minimize the driving power, and design variables are geometrical parameters of the mechanism.

In this paper, we first describe a monolithic design of the micropump, then modeling and optimization processes are described.

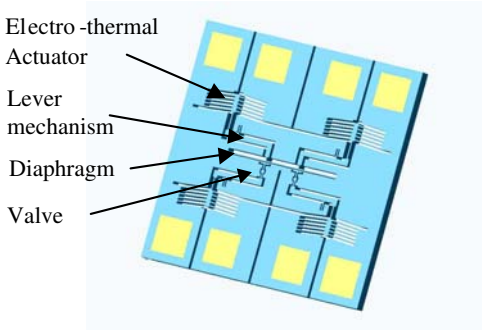

Figure 1: Illustration of an In-Plane Micropump.

2 In-Plane Micropump

2.1 Fabrication of Micropump

A monolithic silicon micropump is illustrated in Figure 1. The pump die is composed of electrothermal actuators, lever mechanisms, a pump diaphragm, and check valves. The actuator consists the ribs of thin silicon, so called V-beam, expands by means of Joule electrical resistance heating. When electrical voltage is applied to the actuator, the force caused by the rib's expansion pulls (or pushes) a rigid bar that is pivoted by a thin flexible bar. The bars act as a lever mechanism to amplify the motion of the actuator. Single or multiple actuators can be used to add force, and this figure shows the case of two thermal actuators for a diaphragm. The magnitude of the diaphragm deflection affects the intake

volume and the compression ratio, therefore a flexible diaphragm is necessary in addition to a large stroke.

The pump die is covered with a glass plate to enclose fluidic flow. A few micron step structure is engraved on the cover plate to allow small gaps between the plates and moving parts of the pump layer. Through-holes in a cover plate are used for the electrical interconnections of the pump, and backside through-holes are used for fluidic interconnection between the pump chamber and the outside.

Either a check valve mechanism or a diffuser can be applied to this pump. Figure 2(a) shows a diffuser at an outlet side (outlet port is not shown). The flow path of an inlet port gradually increases, whereas, the one of outlet port decreases. The inlet flow path is designed to have a lower flow resistance when fluid flows into the pump chamber during the diaphragm expansion, but has higher flow resistance when fluid flows out of the chamber during the diaphragm compression. On the other hand, the output flow path has an opposite characteristic. Accordingly, fluid can be controlled to flow from an inlet port to an outlet port via the pump chamber with repeated diaphragm motions.

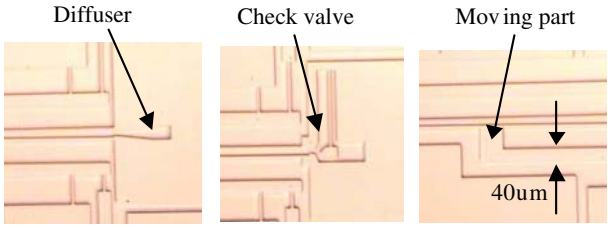

Figure 2: Fabircated diffuser and check valves. (a) Diffuser at an outlet port. (b) A cantilever check valve. (c) Active check valve (actuator is not shown).

Figure 2(b) shows a cantilever check valve mechanism that is passively operated by the pressure difference between the chamber and the ports. With a slender cantilever, each check valve opens and closes the inlet and outlet ports when the diaphragm expands and compresses. As an alternative, an active check valve was also considered as shown in Figure 2(c). It uses the same design of electrothermal actuation. The check valve of an inlet port is powered to open when the diaphragm expands to increase the volume of the pump chamber. The pressure drop due to the increased volume generates flow from the opened inlet port, which is located under the moving part of a valve. The check valve for the outlet port has the same configuration as the inlet check valve, but it opens the port when the pump chamber is compressed.

Figure 3 shows a fabricated micropump structure. In this fabrication, two diaphragms with four actuators are used in symmetry to maximize the compression ratio (only one actuator and two diaphragms are shown).

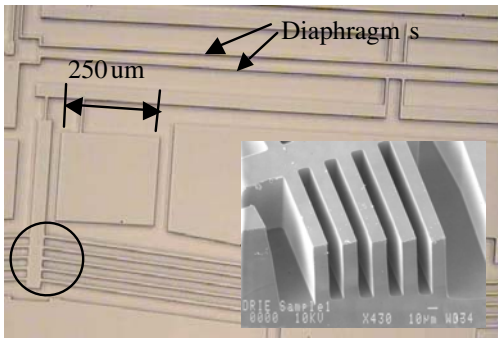

Figure 3: A fabricated micropump structure.

2.2 Structure Characterization

A preliminary experiment was performed to characterize the actuation mechanism of the pump as shown in Figure 4. Actuator dimensions are $12(W) \times 100(H) \times 1200(L)\mu m^3$, and the rib angle is 5.7 . The power consumption is 2W for a serial connection of two actuators, and the deflection of the diaphragm is $30\mu m$ at $12V$. Figure 4(a) shows that the deflection of a diaphragm increases until 16 volts, and decreases afterward as silicon starts to melt at high temperature. In an effort to reduce the driving power, modeling and optimization are used to design the pump actuation structure in the following sections.

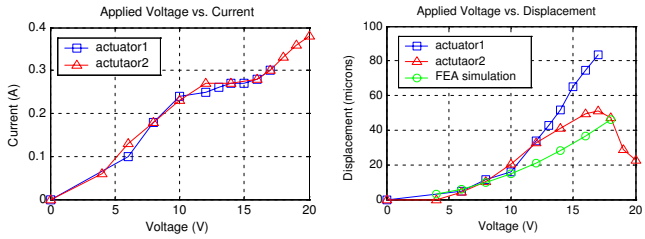

Figure 4: Characterization of pump actuation mechanism. (a) Energy consumption. (b) Displacement of diaphragm.

3 MODELING OF PUMP STRUCTURE

The electrothermal actuator of silicon U and V shape beams have been investigated in [5]–[7]. These models use a one-dimensional heat conduction equation (1),

$$k_s \frac{\partial^2 T(x,t)}{\partial x^2} + J^2\rho - Sk_a \frac{T(x,t) - T_\infty}{gh} = \frac{1}{\alpha}\frac{\partial T(x,t)}{\partial t} \quad (1)$$

where, J, ρ, S, k_s, k_a, g, and h are current density, resistivity, shape conduction factor, thermal conductivity of silicon, thermal conductivity of air, air gap, and

structure thickness respectively. The radiation and convection effects are ignored. Maloney [7] applied the flexibility method [8] to solve the thermal expansion of the one-dimensional V-beam structure of Figure 5. Based upon his result, the thermal expansion δ_A of the V-beam actuator is the function of flexibility coefficient matrices f_{ij} and f_{0i}, where f_{ij} represents the displacement of a point i when a virtual force $X_j = 1$ is applied, and f_{0i} represents the displacement of a point i when all virtual forces are zero except the applied thermal load. Reproduction of this result [7] is summarized as

$$\begin{cases} \delta = \frac{L^2}{24EI}\left(\frac{X_1 L}{2} - 3X_3\right) \\ [X_i] = -\left[f_{ij}\right]^{-1}\left[f_{0i}\right] \\ f_{ij} = \sum_{k=1}^{n}\left[\int_{L_k} \frac{m_{ki}m_{kj}}{EI_k}dx + \frac{L_k n_{ki} n_{kj}}{EA_k}\right] \\ [f_{0i}] = \begin{bmatrix} L & - & L & 0 \end{bmatrix}^T \end{cases} \quad (2)$$

where, $[X_i]$ is a 3×1, and f_{ij} is a 3×3 matrix.

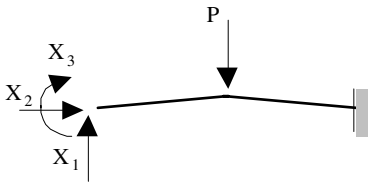

Figure 5: Silicon V-beam actuator with virtual force X_i.

The flexibility method [8] is applied to obtain the stiffness of a V-beam structure. When an external force P is applied to a V beam structure, the displacement due to this force is

$$f_{0i}^P = \begin{bmatrix} \frac{5L^3}{48EI} + \frac{L\theta^2}{EA} & \frac{L^3\theta}{EI} - \frac{L\theta}{EA} & -\frac{L^2}{8EI} \end{bmatrix}^T \quad (3)$$

and the spring coefficient K_A of the V-beam is,

$$K_A = \left[\frac{L^2}{24EI}\left(\frac{X_1^P L}{2} - 3X_3^P\right)\right]^{-1} \quad (4)$$

where, $X_i^P = \left[f_{ij}\right]^{-1}\left[f_{0i}^P\right]$.

Figure 6 illustrates the simplified beam model of a pump, and equations (5,6,7,8) describe corresponding spring constants of the mechanism. K_1 and K_3 relate the displacement of L_5 and L_1 respectively when force is applied at L_1. K_2 and K_4 relate the displacement of L_5 and L_1 respectively, when force is applied at L_5. When the beams L_2 and L_3 are designed to have a high moment of inertia, i.e. $I_2, I_3 \gg I_4$ deflection is mainly created by the bending of the beam L_4.

$$K_1 = \left[\frac{L_2 L_3 L_4}{EI_4} - \frac{L_4}{EA_4}\right]^{-1} \quad (5)$$

$$K_2 = \left[\frac{L_3^3}{3EI_3} + \frac{L_3^2 L_4}{EI_4} + \frac{L_4}{EA_4} + \frac{L_5}{EA_5}\right]^{-1} \quad (6)$$

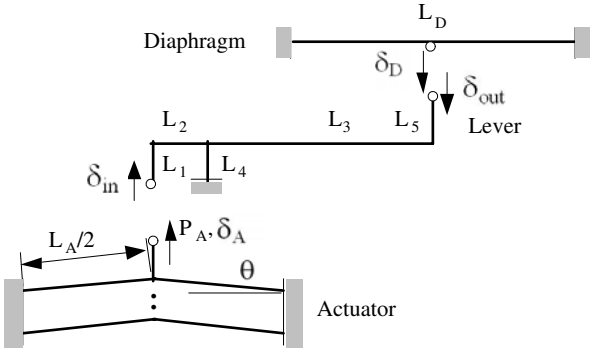

Figure 6: Illustration of pump mechanism as beam structures.

$$K_3 = \left[\frac{L_2^2 L_4}{EI_4} + \frac{L_2^3}{3EI_2} + \frac{L_4}{EA_4} + \frac{L_1}{EA_1}\right]^{-1} \quad (7)$$

$$K_4 = \left[\frac{L_2 L_3 L_4}{EI_4} + \frac{L_4}{EA_4}\right]^{-1} \quad (8)$$

When δ_{out} defines the displacement of output beam L_5 without the diaphragm having any effect, diaphragm deflection δ_D changes the output displacement $\delta_{out} = \delta_{out} - \delta_D = \frac{K_D}{K_2}\delta_D$, where $K_D = \left[\frac{L_D^3}{4 \cdot 48EI}\right]^{-1}$. By substitution of $\delta_{out} = \frac{P_A}{K_1}$, the diaphragm displacement due to the applied force P_A becomes

$$\delta_D = \frac{K_2}{(K_2 + K_D)K_1} P_A. \quad (9)$$

Also, the force from the deflection of the diaphragm react against the actuation force P_A. When δ_{in} defines the displacement of the input beam L_1 without the diaphragm deflection, the actual displacement with the diaphragm deflection $\delta_{in}^{'}$ is $\delta_{in} - \quad \delta_{in} = \frac{P_A}{K_3} - \frac{K_D}{K_4}\delta_D$. Substitution of δ_D using equation (9) gives

$$\delta_{in}^{'} = \frac{P_A}{K_{eq}} \quad (10)$$

where, $K_{eq} = \left[\frac{1}{K_3} - \frac{K_D K_2}{K_4 K_1 (K_2 + K_D)}\right]^{-1}$.

From the force equilibrium condition at the input beam L_1, i.e. $K_{eq}\delta_{in}^{'} = K_A \quad \delta_{in}$, and the actuator displacement condition $\delta_A = \delta_{in}^{'} + \quad \delta_{in}$, the actuation force is determined as

$$P_A = K_A \quad \delta_{in} = K_A \frac{K_{eq}\delta_a}{K_{eq} + K_a}. \quad (11)$$

4 OPTIMIZATION

The optimization goal of this study is to minimize driving power, while achieving a desired pumping stroke and force. As shown in equation (13), the cost function

$f(\mathbf{x})$ is driving power, $V = voltage$, $I = current$ and the optimization variables are,

$$\mathbf{x} = [L_A, \ _A, n_A, V_A, L_2, L_3, L_D] \tag{12}$$

where, n_A, and V_A are number of the V-beams and applied voltage respectively.

$$\begin{aligned} &\underset{x}{\text{Minimize}}\, f(\mathbf{x}) \\ &\qquad f(\mathbf{x}) \ = \ \text{VI} \\ &\text{subject to} \\ &\delta_{Diaphragm} \ \geq \ \delta_{desired} \\ &P_{Diaphragm} \ \geq \ P_{desired} \\ &\qquad T_{Actuator} \ \leq \ T_{limit}. \end{aligned} \tag{13}$$

In this optimization, two parameters, $thickness = 100\mu m$ and $width = 10\mu m$ are fixed as fabrication constraints. Also, the L_4 is fixed to $100\mu m$, because ideally, a longer beam allows greater deflection in the boundary of yield strength. Desired displacement $\delta_{desired} = 30\mu m$, force $F_{desired} = 5mN$ and limit of temperature $T_{limit} = 800K$ are given as inequality conditions. The optimization was performed by Matlab's constrained optimization tool, and its result was shown in Figure 4.

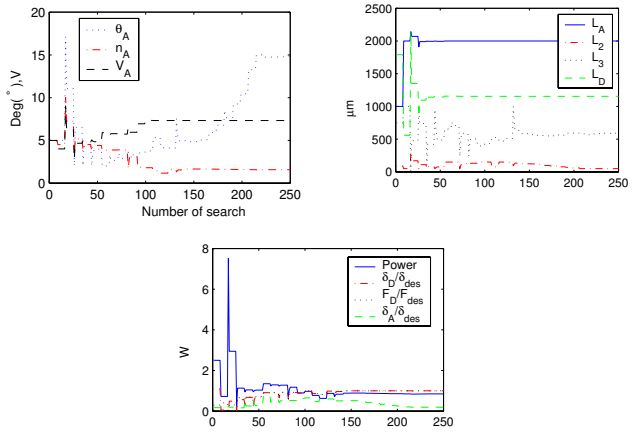

Figure 7: Optimization result of pump actuation structure. (a) Angle, number of ribs and applied voltage. (b) Length of beams. (c) Power, desired displacement and force.

Compared to typical V-beam actuators that use very small angle ($_A = 2 \sim 5$), the optimization result gives a larger angle $_A = 15$. The larger angle makes the actuator stiffer so that the actuator can withstand the reaction force of the lever mechanism. However, as the angle becomes larger, the actuator displacement δ_A becomes smaller. This problem can be solved by making L_2 smaller, while desired displacement is maintained. The driving power is optimized to $1W$ from an initial value $2W$, and it is regarded that multiple solutions exist since the power remained almost constant after 120 iterations.

5 CONCLUSION

A novel, monolithic micropump design was introduced. This approach offers the advantages of embedded actuation and reduced fabrication complexity. We formulated the design of pump actuation structure as an optimization problem by the use of the electrothermal V-beam actuator and lever amplifying mechanism. The result of this work shows that pump driving power can be reduced with optimized micropump structure design. Further study on optimization including fluid flow in the pump is on going, in addition to prototyping.

ACKNOWLEDGEMENT

This work was supported by the Infotonics Technology Center under grant No. DE-FG02-02ER63410.A000 from the US Department of Energy.

REFERENCES

[1] R. Linnemann, P. Woias, C.-D. Senfft, and J.A. Ditterich, "A self-priming and bubble-tolerant piezoelectric silicon micropump for liquids and gases," Proceedings on The Eleventh Annual International Workshop on Micro Electro Mechanical Systems, pp. 532-537, 1998.

[2] F.K. Forster, R.L. Bardell, M.A. Afromowitz, N.R. Sharma, and A. Blanchard, "Design, fabrication and testing of fixed-valve micro-pumps," Proceedings of the ASME Fluids Engineering Division, pp. 39-44, 1995.

[3] C. Grosjean and Y.-G. Tai, "A thermopneumatic peristaltic micropump," International Conference on Solid-State Sensors and Actuators, 1999.

[4] D. Maillefer, S. Gamper, B. Frehner, and P. Balmer, "A high-performance silicon micropump for disposable drug delivery systems," The 14th IEEE International Conference on MEMS, pp. 413-417, 2001

[5] L. Lin and M. Chiao, "Electrothermal responses of lineshape microstructures," Sensors and Actuators, 55, pp.35-41, 1996

[6] Q. Huang and N.K.S. Lee, "Analysis and design of polysilicon thermal flexure actuator," J. Micromech. Microeng., 9, pp.64-70, 1999.

[7] J.M. Maloney, D.L. DeVoe, and D.S. Schreiber, "Analysis and design of electrothermal actuators fabricated from single crystal silicon," in Proc. Micro-Electro-Mechanical-Systems (MEMS)-ASME 2000, pp.233-240, 2000.

[8] J. Oden, "Mechanics of Elastic Structures," McGraw-Hill, New York, 1967.